Observational Study

Medicine®

OPEN

Multimodality imaging-based evaluation of Rosai–Dorfman disease in the head and neck

A retrospective observational study

Qinggang Xu, MD[a,*], Liping Fu, MD[b], Chengyao Liu, MD[c]

Abstract

Rosai–Dorfman disease (RDD) is an uncommon benign entity characterized histologically by lymphatic sinus dilatation due to histiocyte proliferation. This study was performed to delineate its imaging features, reviewed retrospectively in 12 patients (8 women and 4 men, mean age 58.2 years [range 27–84]) with pathologically confirmed RDD in the head and neck. The location, involvement, and imaging characteristics (CT, magnetic resonance imaging (MRI), and PET/CT) of all lesions were evaluated. Signal intensity on MRI images was compared to gray matter (orbital RDD) and adjacent muscle (sinonasal and cervical RDD). RDD in the head and neck involved multiple sites, primarily the sinonasal cavity (n = 7), neck (n = 3), and orbit (n = 1), with one case of simultaneous involvement of the sinonasal cavity, orbit, and neck. With sinonasal involvement, MRI signal intensity of the involved areas was isointense or slightly hyperintense relative to adjacent muscle on T1WI images and heterogeneous on T2WI images; with lacrimal involvement, it was isointense relative to gray matter on T1- and T2-weighted images; and with neck involvement, it was isointense relative to muscle on T1WI images and relatively hyperintense on T2WI images, with homogenous postcontrast enhancement in all sites of involvement. The lesions on CT were observed as enhancing masses with or without bony destruction. PET/CT showed hypermetabolism in one lesion in the neck. RDD is a rare disorder with multiple sites of involvement in the head and neck. Concomitant cervical lymphadenopathy with extranodal masses assisted by multimodal imaging may be useful in the diagnosis of RDD.

Abbreviations: CT = computed tomography, DCE = dynamic contrast enhancement, FOV = field of view, FSE = fast spin-echo, FSPGR = fast spoiled gradient echo, MRI = magnetic resonance imaging, NEX = number of excitation, PET/CT = positron emission tomography/computed tomography, RDD = Rosai–Dorfman disease, SE = spin-echo, SHML = sinus histiocytosis with massive lymphadenopathy, T1WI = T1-weighted image, T2WI = T2-weighted image, TE = echo time, TICs = time-intensity curves, TR = repetition time.

Keywords: computed tomography, head and neck, magnetic resonance imaging, positron emission tomography/computed tomography, Rosai–Dorfman disease

1. Introduction

Rosai–Dorfman disease (RDD), also known as sinus histiocytosis with massive lymphadenopathy (SHML), is a rare but well-defined clinicopathologic entity first described in 1969,[1] with predominant frequency in children, adolescents, and young adults and a slight predominance in men.[2,3] It is characterized histologically by lymphatic sinus dilatation due to histiocyte proliferation, and it frequently mimics a malignant neoplasm, which often leads to inappropriate treatment of this benign but often progressive disease. The most common presentation is massive bilateral painless cervical lymphadenopathy. Extranodal involvement of RDD in the head and neck has been documented in 43% of patients and usually indicates worse prognosis.[4] The most frequent extranodal sites in the head and neck include the paranasal sinuses and nasal cavity, orbit, parotid gland, and middle ear.[5]

The disease rarity, broad differential considerations, and nonspecific imaging findings are why RDD is not often diagnosed in the head and neck. Adding more challenge to the diagnosis, the clinical course of this entity is unpredictable, with episodes ranging from spontaneous regression to protracted periods of stable lymphadenopathy and the less frequent observation of progressive lymphadenopathy. Furthermore, the symptoms of extranodal involvement in the head and neck region are often nonspecific in approximately 75% of patients.

All these difficulties motivated us to perform a retrospective analysis of the clinical experience at our institution to better delineate the imaging features of extranodal involvement in the head and neck, which will contribute to future differential diagnostic studies of RDD. Here we present the imaging findings for a case series of pathologically confirmed RDD in the head and neck in order to increase the familiarity with this entity and further define its imaging findings.

Editor: Rimas Vincas Lukas.

Funding: This study was financially supported by the National Natural Science Foundation of China (no. 81201075).

The authors alone are responsible for the content and writing of the paper.

The authors have no conflicts of interest to disclose.

[a] Department of Radiology, Beijing Tongren Hospital, Capital Medical University, [b] Department of Nuclear Medicine, General Hospital of the Chinese People's Liberation Army and Military Medical Postgraduate College, [c] Department of Otorhinolaryngology, Beijing Tongren Hospital, Capital Medical University, Beijing, China.

[*] Correspondence: Qinggang Xu, Department of Radiology, Beijing Tongren Hospital, Capital Medical University, Beijing 100730, China (e-mail: xuqinggangcn@163.com).

Medicine (2017) 96:51(e9372)

Received: 6 June 2017 / Received in final form: 28 November 2017 / Accepted: 29 November 2017

http://dx.doi.org/10.1097/MD.0000000000009372

2. Materials and methods

An electronic medical record review, approved by the Institutional Review Board revealed 12 patients who presented pathologically confirmed RDD in the head and neck between 2008 and 2016.

Available imaging data for the 12 patients were from computed tomography (CT) for 4 patients, magnetic resonance imaging (MRI) for 3, both CT and MRI for 4, and both MRI and PET/CT for 1. Participants lay supine inside the scanner and heads were restrained with padding behind the neck. During the whole scanning process, participants were required to stay still.

2.1. CT

Axial unenhanced and contrast-enhanced CT was performed with a 64-MDCT scanner (Philips Brilliance, Best, Netherlands; section thickness, 2.0 mm; field of view [FOV] 18×18 cm; 140 kV; 200 mA/slice). For contrast-enhanced CT, 100 mL iopamidol injection (30 g (I)/100 mL/bottle, 1 mL/kg) was injected at 3 to 4 mL/s.

2.2. MRI

All patients had undergone MRI with 8-channel head coil, performed with a 1.5 or 3.0 T MRI imaging scanner (Signa TwinSpeed; GE Healthcare, Milwaukee, WI). The standard institutional imaging protocol for the 1.5/3.0 T scanner used for 7 patients included high-resolution spin-echo (SE) T1-weighted (T1WI) and fast spin-echo (FSE) T2-weighted (T2WI) imaging with 0.5 mm spacing, 5 mm sections, 2 to 4 number of excitation (NEX), 180×220 mm FOV, and a 256×256 matrix. SE T1WI imaging acquisition parameters were time of repetition (TR) 400.0 to 600.0 milliseconds, and time of echo (TE) 15.0 to 20.0 milliseconds. FSE T2WI imaging acquisition parameters were TR 2000.0 to 4000.0 milliseconds, and TE 80.0 to 120.0 milliseconds. Pregadolinium T1WI and T2WI images in 2 planes (axial plus coronal or sagittal) and frequency-selective fat-suppressed axial postgadolinium T1WI images were acquired for all patients. Gadopentetate dimeglumine (0.1 mmol/kg, Magnevist; Bayer Schering Pharma, Berlin, Germany) contrast agent was injected at 2.0 mL/s through a 21-gauge intravenous line with a power injector. Before postcontrast MRI images were obtained, 2 patients underwent dynamic contrast enhancement (DCE)-MRI with 3D-fast spoiled gradient echo (FSPGR), with the acquisition parameters TR 8.4 milliseconds, TE 4.0 milliseconds, flip angle 15°, FOV 220×220 mm, matrix size 256×160, slice thickness 3.2 mm with 0 spacing and 5-minute acquisition time. During DCE-MRI, 12 sequential 13-second images with 12-second intervals were acquired as follows: one control image before injection of contrast agent and 11 images during and after injection. The time-intensity curves (TICs) were used for analyzing the enhancement patterns.

2.3. PET/CT

^{18}F-FDG PET/CT images (Biograph Truepoint 64, Siemens Healthcare, Erlangen, Germany) were obtained 50 minutes after intravenous injection of ^{18}F-FDG at 4.81 to 5.55 MBq (0.13–0.15 mCi)/kg and the covered range was from the top of the skull to the mid-thigh. The participant was instructed to fast for 4 to 6 hours and blood glucose was measured before injection to ensure that levels were within the reference range. A 14-minute PET acquisition (10-minute/5 bed for the trunk and 4-minute/bed for brain) was performed in 3D acquisition mode. Data obtained from CT acquisition (120 kV, 100 mA, and 3.75-mm slice thickness) were used for attenuation correction of PET emission data.

3. Results

Table 1 provides the demographic, clinical, and imaging details of the 12 patients with RDD (8 women and 4 men; mean age 58.2 years [range 27–84] at diagnosis). The lesions appeared in multiple sites, mainly in the sinonasal cavity and nasopharynx (n = 7), neck (n = 3), and orbit (n = 1) with one case (case 5) of simultaneous involvement of the sinonasal cavity, orbit, and neck. Here we discuss the involvements in detail.

3.1. Nasal cavity and paranasal sinus involvement

There were 8 cases of sinonasal cavity involvement. The lesions were multifocal and the most common sites were the nasal cavity, maxillary sinus, and ethmoidal sinuses. In patient 2, choana was involved, with extension into the sphenopalatine foramen. In

Table 1

Demographic, clinical, and imaging characteristics of patients with Rosai–Dorfman disease.

Patient No.	Age	Sex	Symptoms	Imaging findings
1	80	F	Hoarseness	CT: enhancing mass in the bilateral glottis, paralaryngeal space; supramediastinal LN enlargement
2	40	M	Nasal obstruction, epistaxis	CT: mass in the right sphenoidal sinus, choana with extension into sphenopalatine foramen
3	84	M	Nasal obstruction	MRI: enhancing masses in the bilateral nasal cavity, ethmoidal sinuses and left maxillary sinuses
4	68	F	Swelling in right cheek	CT: opacification of right maxillary sinus
5	28	F	Nasal obstruction, facial pain; hoarseness	CT: masses in the nasal cavity, orbit, nasopharynx, hard palate involvement with extension into pterygopalatine fossa; masses in the left scoop epiglottis plica and glottis; bilateral neck LNs enlargement
6	76	F	Nasal obstruction	MRI: enhancing masses in the nasal cavity bilaterally
7	72	M	Right eye swelling	MRI: right lacrimal gland and orbital mass
8	52	F	Hoarseness	CT and MRI: enhancing mass in the right glottis, paralaryngeal space; neck LNs
9	48	F	Nasal obstruction, hyposmia	CT and MRI: enhancing masses in the bilateral nasal cavity, nasopharynx with bony destruction; neck LNs
10	55	F	Neck swelling, hoarseness	MRI and PET/CT: enhancing (hypermetabolic) mass in the left glottis, paralaryngeal space; neck LNs
11	71	M	Nasal obstruction	CT and MRI: enhancing masses in the right nasal cavity without bony destruction; neck LNs
12	27	F	Nasal obstruction	CT and MRI: enhancing masses in the bilateral nasal cavity, nasopharynx with bony destruction; neck LNs enlargement

CT = computed tomography, LN = lymph node, MRI = magnetic resonance imaging, PET/CT = positron emission tomography/computed tomography.

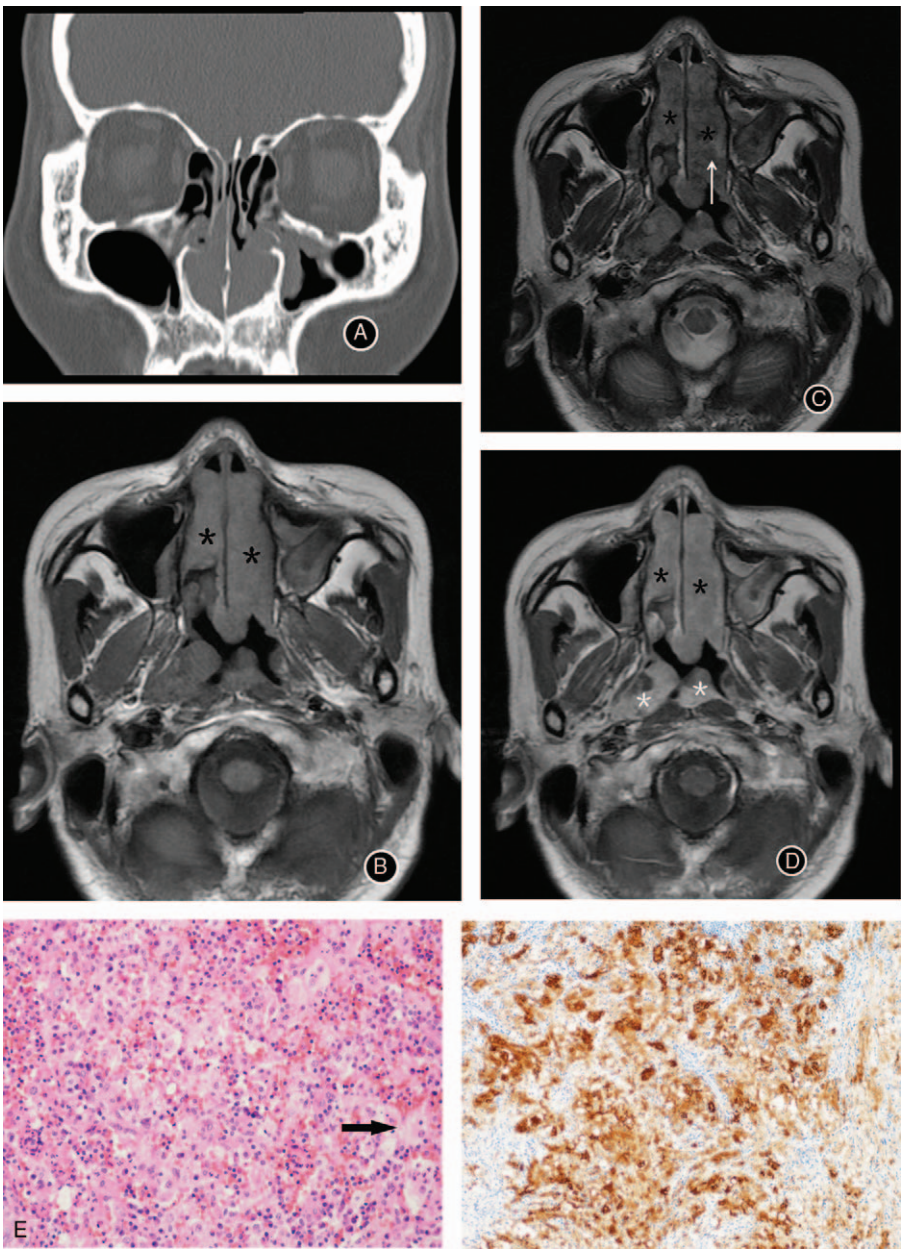

Figure 1. Rosai–Dorfman disease (RDD) in a 48-year-old woman with nasal obstruction and sinonasal disease. (A) Coronal reformat of CT scan in bone algorithms reveals soft-tissue mass in bilateral nasal cavity with middle and inferior turbinate reabsorption versus erosion. (B) Axial T1-weighted image shows an irregular mass (*) involving the bilateral cavity and nasopharynx mildly hyperintense relative to muscle tissue. (C) On axial T2WI imaging, the lesion shows hypointense areas (arrow) within a background of hyperintensity (*) relative to adjacent muscle tissue. (D) Gadolinium-enhanced axial image shows diffuse enhancement of masses, which are slightly heterogeneous (*), following the pattern of heterogeneity on the T2-weighted image. (E) Left: Histopathological images of the lesion. High-power photomicrograph shows distinctive histiocytes of RDD that are large with abundant and finely granular pink cytoplasm and relatively large nuclei with open chromatin and distinct nucleoli. Images show engulfment of intact lymphocytes and plasma cells by the large histiocytes, a phenomenon known as emperipolesis (arrow) (hematoxylin–eosin stain, original magnification: Å~300). Right: Positive for S-100 protein (immunohistochemistry).

patient 5, the nasopharynx and hard palate were also involved, with extension into the pterygopalatine fossa.

Contrast-enhanced CT images were available for 3 patients, who showed homogeneously enhanced soft masses with no calcification in the sinonasal cavity, and one of the nasal lesions showed middle and inferior turbinate reabsorption versus erosion (Fig. 1A). MRI images revealed 5 lesions that were slightly hyperintense relative to adjacent muscle on T1WI images (Fig. 1B) and heterogeneous on T2WI images with avid homogeneous enhancement on gadolinium enhancement (Fig. 1D). Remarkably, the lesions showed hypointense areas within a background of hyperintensity on T2-weighted images (Fig. 1C).

3.2. Cervical involvement

Four patients with RDD had cervical involvement with or without lymph node enlargement. The main involved sites were the glottis and paralaryngeal space. CT images were available for 3 patients and showed homogeneously enhanced masses. The MRI characteristics of the lesions (n = 2) were similar to findings

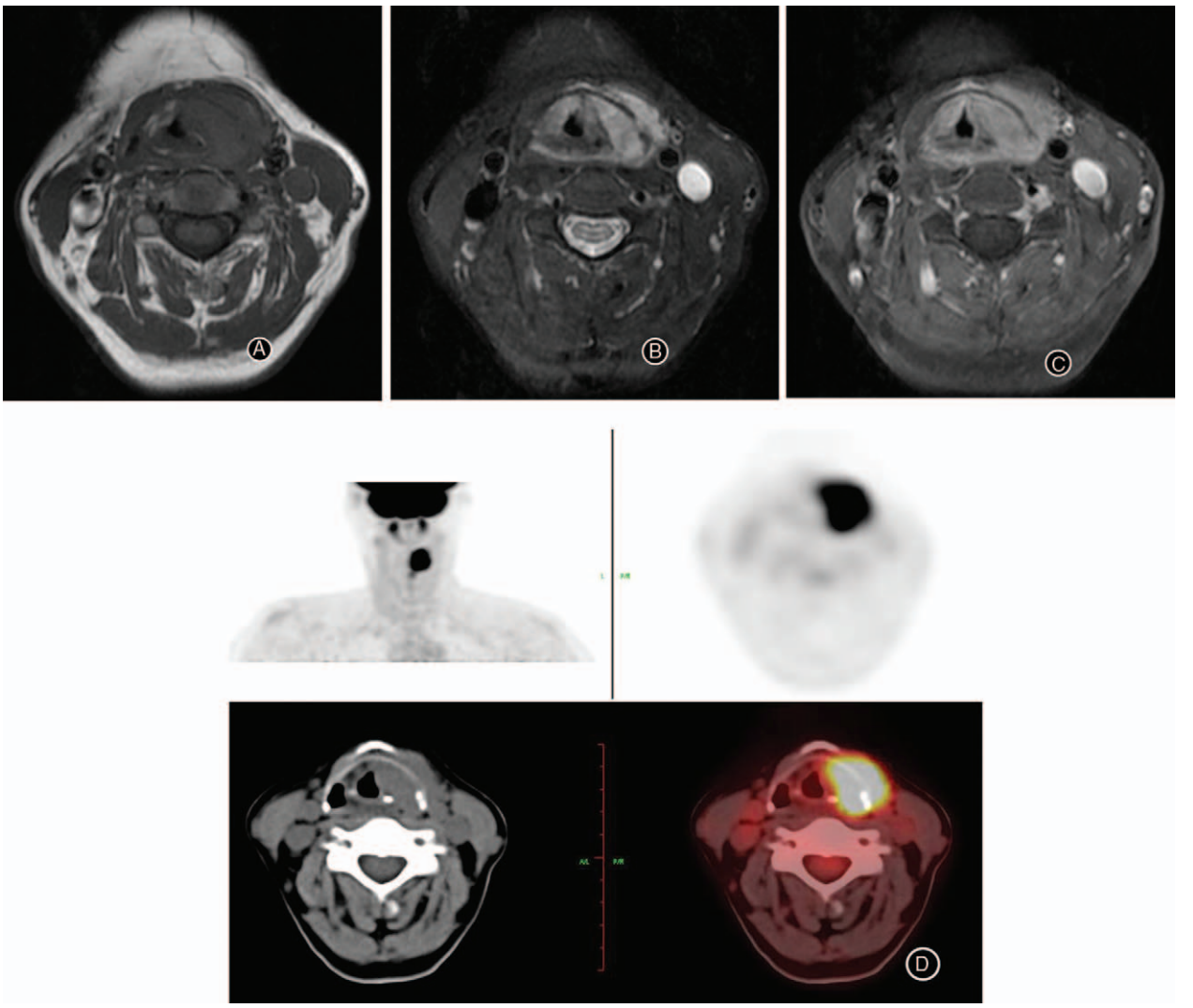

Figure 2. RDD in a 55-year-old woman with neck swelling and hoarseness. (A) Axial T1-weighted MRI images show mass involving the left glottis, paralaryngeal space, and prelaryngeal muscles beyond the confined of the thyroid cartilage, with isointensity relative to muscle tissue. (B) The lesion is relatively hyperintense on T2WI with fat suppression. (C) Axial contrast-enhanced T1-weighted image with fat saturation shows avid and homogeneous contrast enhancement. (D) Corresponding PET/CT image confirms hypermetabolic nature of lesions.

elsewhere: signal intensities similar to that of muscle on T1-weighted sequence (Fig. 2A) and relative hyperintensity on T2WI image (Fig. 2B) with homogeneous enhancement (Fig. 2C). PET/CT (patient 10) revealed that the left paralaryngeal space was hypermetabolic, with maximum standardized uptake value (SUVmax) up to 13.3 (Fig. 2D).

3.3. Lacrimal gland involvement

One patient (patient 7) had lacrimal gland involvement. MRI revealed right lacrimal gland enlargement with intermediate signal intensity on T1- and T2-weighted images and intense homogeneous enhancement (Fig. 3A–C). DCE-MRI showed rapid initial enhancement followed by a wash-out phase (Fig. 3D).

Pathologically, the lesion showed abundant plasma cells and sinus histiocytes containing phagocytized normal lymphocytes within an abundant cytoplasm, including large, pale pathognomonic histiocytes that exhibited emperipolesis (Fig. 1E). Further immunohistochemical staining showed large histiocytes positive for S-100 and CD-68 protein but negative for CD1a protein.

4. Discussion

This was a retrospective analysis of the clinical experience with RDD at our institution to detail the imaging features of RDD with involvement in the head and neck. RDD involved multiple sites, primarily the sinonasal cavity, neck, and orbit. With sinonasal involvement, MRI signal intensity was isointense or slightly hyperintense on T1WI images and heterogeneous on T2WI images; with lacrimal involvement, it was isointense on T1- and T2-weighted images; and with neck involvement, it was isointense on T1WI images and relatively hyperintense on T2WI images. CT lesions were observed as enhancing masses with or without bony destruction. PET/CT showed hypermetabolism in one lesion in the neck. Concomitant cervical lymphadenopathy with extranodal masses along with multimodal imaging may be useful in the diagnosis of RDD.

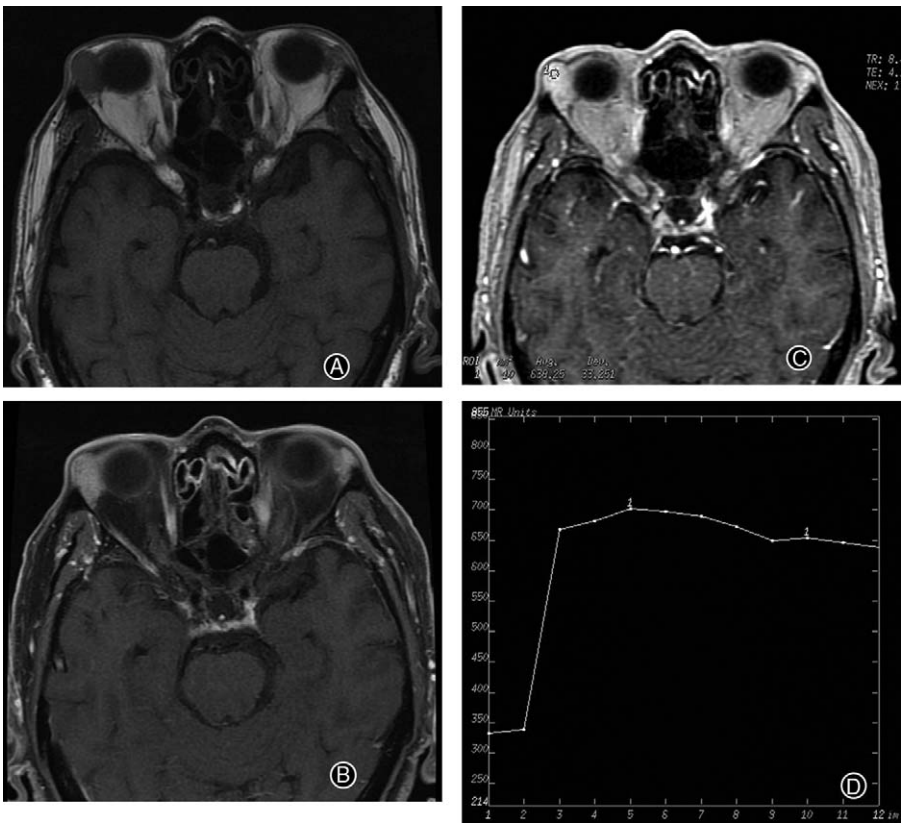

Figure 3. RDD in a 72-year-old man with swelling of the right eye. (A) Axial T1WI image reveals right lacrimal gland mass isointense relative to gray matter. (B) Axial contrast-enhanced T1-weighted image with fat saturation shows homogeneous enhancement. (C) Region of interest placement on axial dynamic contrast enhancement images. Enhancement curve shows rapid initial enhancement followed by a wash-out phase. (D) Time-intensity curves of DCE-MRI.

RDD is an extremely rare and idiopathic benign disease characterized histologically by lymphatic sinus dilatation due to histiocyte proliferation that may feature a racial discrepancy and is reported to be more common in people of African and West Indian background.[6] Its occurrence has frequently been observed after infectious disease, immunodeficiency, autoimmune disease, and a neoplastic process. However, no causes have been confirmed. In most RDD cases, treatment is not necessary. Therapy is required for patients with extranodal RDD and vital organ involvement or with lesions causing life-threatening complications.[7] At present, there is no ideal schema to treat the diverse types of RDD lesions in a similar manner. Multiple strategies of therapy that should be tailored to the individual lesion or patient include radiation therapy, chemotherapy, steroids, and surgery, which have been used with varying success.[2,6–9]

Extranodal RDD is not common, and with more severe fibrosis and fewer histiocytes in lesions, the diagnosis of extranodal RDD is more difficult than that of nodal RDD.[10] Further complicating the diagnosis, up to 85% patients have no significant symptoms with their disease, and patients may manifest extranodal disease in the absence of lymphadenopathy.[11] Hence, we need to better define the appearance of RDD and increase physician awareness of the disease within the differential diagnosis in the head and neck. As well, we need to continue to investigate complementary noninvasive imaging techniques, including CT, MRI, and PET/CT, that can differentiate RDD from the more common diseases in the head and neck.

For this imaging presentation of RDD, we identified some imaging manifestations. The most common was deep cervical lymphadenopathy, present in 7 cases, which is compatible with the original description of the disease.[10,12,13] Multiple sites of involvement were also identified, which confirmed 2 concerns. One was that the lesions can be found in many sites such as nasal cavity, paranasal sinuses and extended canal/foremen, pharynx and its adjacent space, glottis beyond nearby structures, and orbit. The differential diagnosis with malignant tumors should be considered. In this study, CT typically displayed polypoid masses or opacification of the sinonasal cavity, with or without associated osseous erosion. The abnormal soft tissue generally shows associated homogeneous contrast enhancement and increased activity on PET. However, a malignant process cannot completely be ruled out on the basis of these nonspecific findings, by the distribution pattern or the intensity of the contrast accumulation. Therefore, although rare, RDD ought to be considered in the differential diagnosis in cases of massive lymphadenopathy or extranodal manifestations or both. However, multifocal lesions may be found simultaneously in one patient. The imaging manifestations of RDD should not overlap with those of lymphoma. Massive painless bilateral cervical lymph-node enlargement can help in considering RDD, whereas lymphoma may feature enlargement and fusion of lymph nodes. In addition, the splenomegaly and diffused hypermetabolism in bone marrow seen on FDG-PET images may be an indication for lymphoma[14,15] because RDD can seldom cause a whole-body reactive response. Although the uptake of FDG in RDD is not specific,[16] some research highlights that whole-body PET/CT imaging can show the extent of the disease, help with complete staging, provide functional information about disease activity to

guide biopsy, and even be used to monitor the follow-up therapeutic response.[12,17]

Increasing studies have concerned RDD in recent years. However, they were clinical short communications,[9,10,13] basically confirmed previous study findings,[11,18,19] or contained limited imaging information.[20] Our MRI investigations revealed some characteristic signals in lesions. With sinonasal involvement, the signal intensity of involved areas was slightly hyperintense relative to adjacent muscle on T1WI images and heterogeneous on T2WI images, with avid homogeneous enhancement on gadolinium-enhanced images. Remarkably, the lesions showed hypointense areas within a background of hyperintensity on T2-weighted images, believed to be due to free radicals released by inflammatory macrophages.[20,21] This signal description differed from previous descriptions,[21,22] in which sinonasal RDD appeared isointense relative to gray matter on T1WI and T2WI images. This difference is believed to be the choice of media (gray matter or muscle). However, a typical representation of hypointensity regardless of calcification on T2-weighted images can suggest RDD.

The major limitation of this study was that the number of cases was too small to provide definitive quantitative estimates of RDD. Our conclusions need to be further evaluated with data from more patients with RDD.

In conclusion, RDD in the head and neck is an uncommon benign pseudolymphomatous entity with a variety of imaging manifestations. The disease tends to be multifocal and should be included in the differential diagnosis when encountered in the neck with painless lymphadenopathy. Because extranodal RDD in clinical presentations is nonspecific and massive cervical lymph node involvement is not always present, this retrospective study indicates that beyond cervical lymphadenopathy, multiple sites of involvement or a typical representation of hypointensity regardless of calcification on T2-weighted images should be considered for a RDD diagnosis. Advanced MRI and PET/MRI techniques such as conventional cross-sectional imaging with high fractional anisotropy, a low apparent diffusion coefficient, mild blooming on susceptibility-weighted imaging images and decreased perfusion may help with easier diagnosis of RDD.

Acknowledgment

The authors thank Judith Gatton Prats, University of Kentucky Writing Center, for help in manuscript editing.

References

[1] Rosai J, Dorfman RF. Sinus histiocytosis with massive lymphadenopathy. A newly recognized benign clinicopathological entity. Arch Pathol 1969;87:63–70.

[2] Maia RC, de Meis E, Romano S, et al. Rosai-Dorfman disease: a report of eight cases in a tertiary care center and a review of the literature. Braz J Med Biol Res 2015;48:6–12.

[3] Lim R, Wittram C, Ferry JA, et al. FDG PET of Rosai-Dorfman disease of the thymus. AJR Am J Roentgenol 2004;182:514.

[4] Geara AR, Ayoubi MA, Achram MC, et al. Rosai-Dorfman disease mimicking neurofibromatosis: case presentation and review of the literature. Clin Radiol 2004;59:625–30.

[5] Juskevicius R, Finlay JL. Rosai-Dorfman disease of the parotid gland, cytologic and histopathologic findings with immunohistochemical correlation. Arch Pathol Lab Med 2001;125:1348–50.

[6] Dalia S, Sagatys E, Sokol L, et al. Rosai-Dorfman disease: tumor biology, clinical features, pathology, and treatment. Cancer Control 2014;21: 322–7.

[7] Pulsoni A, Anghel G, Falcucci P, et al. Treatment of sinus histiocytosis with massive lymphadenopathy (Rosai-Dorfman disease): report of a case and literature review. Am J Hematol 2002;69:67–71.

[8] Mantilla JG, Goldberg-Stein S, Wang Y. Extranodal Rosai-Dorfman Disease: clinicopathologic series of 10 patients with radiologic correlation and review of the literature. Am J Clin Pathol 2016;145: 211–21.

[9] Duan HG, Zheng CQ, Wang DH, et al. Extranodal sinonasal Rosai-Dorfman disease: a clinical study of 10 cases. Eur Arch Otorhinolaryngol 2015;272:2313–8.

[10] Yajima M, Nakajima K, Hirato J, et al. Extranodal soft tissue Rosai-Dorfman disease of the head and neck and its diagnostic difficulty. Auris Nasus Larynx 2016;43:345–9.

[11] Ottaviano G, Doro D, Marioni G, et al. Extranodal Rosai-Dorfman disease: involvement of eye, nose and trachea. Acta Otolaryngol 2006; 126:657–60.

[12] Fu L, Liu M, Song Z, et al. 18F-fluoro-deoxyglucose positron emission tomography/computed tomography scan findings in Rosai-Dorfman disease with IgG4-positive plasma cell infiltration mimicking breast malignancy: a case report and literature review. J Med Case Rep 2012;6:411.

[13] Al-Moosa AJ, Behbehani RS, Hussain AE, Ali AE. Orbital Rosai–Dorfman disease in a five-year-old boy. Middle East Afr J Ophthalmol 2011;18:323–5.

[14] El Karak F, Bou-Orm IR, Ghosn M, et al. PET/CT scanner and bone marrow biopsy in detection of bone marrow involvement in diffuse large B-cell lymphoma. PLoS ONE 2017;12:e0170299.

[15] Shah HJ, Keraliya AR, Jagannathan JP, et al. Diffuse large B-cell lymphoma in the era of precision oncology: how imaging is helpful. Korean J Radiol 2017;18:54–70.

[16] Metser U, Even-Sapir E. Increased (18)F-fluorodeoxyglucose uptake in benign nonphysiologic lesions found on whole-body positron emission tomography/computed tomography (PET/CT): accumulated data from four years of experience with PET/CT. Semin Nucl Med 2007;37: 206–22.

[17] Albano D, Bosio G, Bertagna F. 18F-FDG PET/CT follow-up of Rosai-Dorfman disease. Clin Nucl Med 2015;40:e420–2.

[18] Sennes L, Koishi H, Cahali R, et al. Rosai-Dorfman disease with extranodal manifestation in the head. Ear Nose Throat J 2004;83:844–7.

[19] Azoulay R, Brisse H, Fréneaux P, et al. Lacrimal location of sinus histiocytosis (Rosai-Dorfman-Destombes disease). AJNR Am J Neuroradiol 2004;25:498–500.

[20] La Barge DV, Salzman KL, Harnsberger HR, et al. Sinus histiocytosis with massive lymphadenopathy (Rosai-Dorfman disease): imaging manifestations in the head and neck. AJR Am J Roentgenol 2008; 191:W299–306.

[21] Zhu H, Qiu L-H, Dou Y-F, et al. Imaging characteristics of Rosai-Dorfman disease in the central nervous system. Eur J Radiol 2012; 81:1265–72.

[22] Raslan OA, Schellingerhout D, Fuller GN, et al. Rosai-Dorfman disease in neuroradiology: imaging findings in a series of 10 patients. AJR Am J Roentgenol 2011;196:W187–93.